Long-term slope instability induced by the reactivation of Mass Transport Complexes: An underestimated geohazard on the Norwegian continental margin

Song Jing[1,2], Tiago M. Alves[2], Kamaldeen O. Omosanya[3,4], Wei Li[1,*]

[1] CAS Key Laboratory of Ocean and Marginal Sea Geology, South China Sea Institute of Oceanology, Chinese Academy of Sciences, Guangzhou 510301, China

[2] 3D Seismic Lab, School of Earth and Environmental Sciences, Cardiff University, Main Building, Park Place, Cardiff, CF10 3AT, United Kingdom

[3] Oasisgeoconkonsult, 7052 Trondheim, Norway

[4] Norwegian University of Science and Technology, Trondheim, Norway

Corresponding author: Dr. Wei Li (wli@scsio.ac.cn)

ABSTRACT

Submarine landslides are significant geohazards, capable of displacing large volumes of sediment from continental margins to deposit mass-transport complexes (MTCs) and generate offshore tsunamis. However, the reactivation of MTCs after their initial failure has long been overlooked. By analysing high-quality three-dimensional seismic reflection data and seismic attribute maps, as well as comparing the geometry of different MTCs, we investigate the development of long-term slope instability and its hazardous consequences on the northwest flank of the Storegga Slide. Our results demonstrate that the reactivation of MTCs can deform both their inner structure and overlying strata, promoting the formation of sinuous channels and local slope failures on the seafloor. These findings further reveal the MTCs that are underconsolidated or comprise slide blocks may remain unstable for a long time after their initial failure, particularly when affected by slope undercutting and a corresponding reduction in lateral support. This study shows that MTC-prone sequences are more likely to comprise regions of continental slopes with long-term instability and recurring marine geohazards.

Keywords: Storegga Slide; Slope instability; Laterally spread blocks; MTCs' reactivation; Geohazards.

INTRODUCTION

Submarine landslides are a major source of seafloor deformation and hazardous tsunamis, being capable of damaging both subaqueous and coastal infrastructures in single or multiple events (Harbitz et al., 2006; Talling et al., 2007; Sun et al., 2018a). Previous research concerning slope instability processes usually separates major and long-term precondition factors such as high sediment supply, overpressure and slope oversteepening, from short-term triggers that include earthquakes, volcanism and human activity (Leynaud et al., 2009; Urlaub and Hjelstuen, 2020). A comprehensive evaluation of submarine landslide likelihood, landslide distribution, preconditioning factors and any episodic triggers is therefore crucial to a complete assessment of long-term slope instability (Masson et al., 2006; Leynaud et al., 2009).

Mass transport deposits (MTDs) and mass transport complexes (MTCs) are terms used interchangeably in the literature, representing distinct phenomena, scales of analysis, and degrees of instability (Alves et al., 2022). Mass movements in nature can be generalized into a term representing a wide spectrum of deposits, the so-called mass transport complexes (MTCs), particularly when their strata are clearly associated in space and time (Pickering and Hiscott, 2015). Single failure events eroding parts of a continental slope and depositing discrete intervals of failed, convoluted beds, are usually referred to as mass transport deposits (MTDs) (Wang et al., 2017; Shanmugam, 2021). Thus, MTCs are usually thicker and represent long-lasting slope failure when compared with the more episodic, discrete MTDs (Alves, 2015).

MTCs can develop for several millions of years and are usually recognized via the interpretation of seismic and borehole data and outcrop expression in both marine environments and exhumed orogenic belts (Solheim et al., 2005a; Pini et al., 2012; Ogata et al., 2019b). They can be several thousands of cubic kilometers in volume, presenting varied internal kinematic indicators and heterogeneous internal structures (Bull et al., 2009a; Urgeles and Camerlenghi, 2013; Dalla Valle et al., 2015; Moscardelli and Wood, 2016; Omosanya, 2018; Ogata et al., 2019a). After both MTCs and MTDs are deposited, differential compaction processes in their interior can further influence the overlying slope morphology by generating local depressions and fractures near the seafloor (Alves, 2010).

Despite their significance in the geological record, MTCs have seldom been considered in the literature to be the sources, or triggers, of further slope instability. This most likely owes to the limited resolution of seismic reflection data, which could not clearly differentiate MTCs' reactivation from 'syn-failure' depositional features and structures. Nevertheless, the reservoir and seal potentials of MTCs have attracted the energy industry's interest in the past few years, raising important concerns regarding the instability and geohazard potential of large swathes of continental margins in which they occur (Alves et al., 2014, 2022; Cox et al., 2020).

In this study, high-resolution three-dimensional seismic reflection data are used to characterize slope instability in the understudied northwest flank of Storegga Slide on the Norwegian margin, where submarine landslides have occurred during the Quaternary glaciation period (Bryn et al., 2003; Solheim et al., 2005) (Fig. 1a and 1b). Geochronological and bathymetric data have previously highlighted the significance of long-term slope instability in other parts of the Storegga area by recognizing multiple slide scarps and channels in MTCs (Haflidason et al., 2004, 2005). This research further identifies a series of post-failure features associated with MTCs. It shows that MTCs can deform the seafloor well after their initial emplacement, highlighting the presence of long-term instability in the areas where they occur. Together with their triggers and development, this paper shows that the deposited MTCs could still be unstable in long term and may lead to an underestimation of subaqueous geohazards.

DATA AND METHODS

This work uses time- and depth-migrated 3D seismic data and one exploration well (6403/6-1) from the mid-Norwegian margin (Fig. 1a). The seismic data cover 263 km^2 of the northwest flank of the Storegga Slide, over the south Modgunn Arch (gray-shaded area in Fig. 1a). The summit of this arch was drilled by well 6403/6-1, providing lithostratigraphic and wireline information such as formation tops, depth and bulk density of drilled strata. Therefore, relative dates for seismic-stratigraphic units are based, in this work, on seismic-well ties and published information from the Norwegian margin (Berg et al., 2005; Jing et al., 2020).

Seismic interpretation uses Schlumberger Petrel® and includes the compilation of relevant two-way time (TWT) structural and seismic-attribute maps. In order to visualize the multiple MTCs and structures identified on seismic, we compute RMS amplitude, TWT structure and variance maps for key seismic horizons and geological features. TWT structure maps are computed for the seafloor (horizon H1) and glide planes of interest. Slide scarps, fractures, slumped strata, and submarine channels are features with high variance and high RMS amplitude, whereas small-scale MTCs comprise high-relief, low-variance features. The geometry of channels, furrows and blocks, including their sinuosity, dimensions and orientations, are also analyzed in this work.

GEOLOGICAL SETTING

Lithostratigraphy

The study area is located on the northwest flank of the Storegga Slide, at a latitude of around 64°N on the mid-Norwegian margin, where the continental slope rises in two directions, both northeastward and southeastward (Fig. 1a). Based on Exploration Well 6403/6-1, the lithostratigraphy of our study area can be divided into a breakup sequence (below horizon H6 in Fig. 1d) and several post-breakup units above (Jing et al., 2020). The breakup sequence was not deformed by slope instability processes. In contrast, post-breakup units between horizons H6 and H1 were deformed, eroded and evacuated by recurrent slope failures (Figs. 1c and 1d). These post-breakup strata are stratigraphically equivalent to the Brygge, Kai and Naust formations (Fig. 1d).

The Kai and Brygge formations, upper Eocene to upper Pliocene in age and respectively placed between horizons H4-5 and H5-6 (Fig. 1d), are composed of marine claystone with intervals of sandstone, siltstone, limestone and marl (Dalland, 1988). Biogenic ooze, with relatively high porosity and water content - when compared with clay or sand - predominates in these two formations (Lawrence and Cartwright, 2010). Between horizons H1 and H4, the Naust Formation has accumulated from the Early Pleistocene to the present day, comprising alternating glacial and marine deposits (Bryn et al., 2003). Long-term slope instability in the Naust Formation is document by multiple headwall and lateral scarps, channels, and accompanying MTCs (Bryn et al., 2003; Haflidason et al., 2004, 2005; Kvalstad et al., 2005; Baeten et al., 2014). Importantly, these MTCs are potential unstable in the long term due to their high clay content, which prevents the recovery of shear strength after their deposition and allows additional deformation (Lewis et al., 1998; Dellisanti et al., 2008; Camerlenghi and Pini, 2009; Sawyer et al., 2009; Mesri and Huvaj-Sarihan, 2012; Conti et al., 2014).

MTCs near the Storegga area

The structure of MTCs can be recorded by the seismic character and kinematic indicators they present, such as grooves, scarps, fractures and slide blocks (Bull et al., 2009a; Alves, 2015). In the Storegga area, multiple MTCs overlapped each other along with the occurrence of the Storegga Slide complex, including the Slide W, Slide S, Slide R and the Storegga Slide (Bryn et al., 2003; Solheim et al., 2005b) (Figs. 1a, 1c and 1d). Higher on the continental slope, bathymetric and seismic data image several MTCs with slide blocks, correlating with Slides S and R, formed above gentle glide planes with gradients of less than 2° (Gauer et al., 2005; Micallef et al., 2007; Bull et al., 2009b) (Figs. 1c and 1d). At least two types of seismic facies have been observed in these MTCs: a) chaotic to transparent facies with grooves and flow-like features denoting greater transport distances, and b) discontinuous stratified facies comprising slide blocks whose movement was relative limited (Gauer et al., 2005; Solheim et al., 2005a; Micallef et al., 2009; Sawyer et al., 2009).

Slide W

Slide W materializes the oldest failure event of the Storegga Slide complex, having occurred before 1.7 Ma (Bryn et al., 2003; Solheim et al., 2005) (Fig. 1a and 1d). The relief map of its basal glide plane reveals local depressions, previously interpreted as craters or ooze evacuation structures (Riis et al., 2005; Lawrence and Cartwright, 2010). Above the basal glide plane, MTCs with basal striations, inner imbrications and ooze mounds suggest recurrent slope failure during ooze evacuation (Riis et al., 2005; Jing et al., 2022; Omosanya et al., 2022). Except for slide blocks along their sidewalls, these MTCs comprise transparent to chaotic seismic facies (Riis et al., 2005; Lawrence and Cartwright, 2010; Omosanya et al., 2022). On the northwest flank of the Storegga Slide, three craters are observed cutting into the Brygge Formation (C1 to C3 in Omosanya et al., 2022). In study area, these Slide W MTCs have been eroded and removed by subsequent slope failure events, leaving an 'L'-shaped ramp on the modern seafloor (Jing et al., 2020, 2022) (Figs. 1b and 1c).

Slides S and R

Slides S and R occurred in the Storegga area at respectively ~ 0.5 Ma and ~ 0.3 Ma (Berg et al., 2005) (Fig. 1a, 1c and 1d). These two slides comprise debrites and blocks with chaotic to stratified seismic characters (Bryn et al., 2003). In the upper part of these two slides, nearly intact and rotated slide blocks are observed above well-defined glide planes (Bryn et al., 2003; Solheim et al., 2005). Scarp S5 in our study area seems to separate Slides S and R (Fig. 1b, 1c and 1d), but further interpretation indicates that Slide S was capable of triggering the development of Slide R further up on the slope (Bull et al., 2009b). This opens questions about the true relationship between Slides S and R and how their interaction was able to promote long-term slope instability in the study area.

Storegga Slide

The Storegga Slide, as the most recent slope failure of the Storegga Slide complex, affected a total area of 90,000 km^2 since around 8200 ya (Bryn et al., 2003) (Fig. 1a and 1d). Subsequent structures, such as scars, scarps and MTCs, are exposed on the modern seafloor, denoting variable features such as closely spaced blocks along their headwalls and compressional structures (toe thrusts) on the lower part of the continental slope (Haflidason et al., 2005; Bull et al., 2009a). Debris and turbidity channels can be recognized as linear structures with particular seismic characters, such as chaotic seismic reflectors with higher variance and amplitude (Haflidason et al., 2004). Seismic data and sediment cores from the northern flank of the Storegga Slide indicate that local slope failure has continued for ~5000 yrs after its main episode (Haflidason et al., 2004, 2005). This observation once more suggests long-term slope instability in the study area.

Development of MTCs Comprising Slide Blocks

MTCs with closely spaced and tilted coherent blocks are observed on bathymetric and seismic data all over the mid-Norwegian margin, and also near the Storegga Slide, generating a rugged seafloor (Solheim et al., 2005a; Micallef et al., 2007). Below these blocks, seismic and sediment core data reveal a layer-parallel glide plane that propagates at present into intact layers on the upper continental slope after lateral support was lost by the undercutting of the lower continental slope (Locat et al., 2016; Giona Bucci et al., 2022). These layers comprise soft marine clays interbedded with (harder) glacial deposits, resulting in weak layers with lower shear strengths, higher sensitivity and excess pore pressures when compared to the confining strata (L'Heureux et al., 2012; Ogata et al., 2014; Locat et al., 2016; Gatter et al., 2021; Wu et al., 2022).

Propagating glide planes can eventually disrupt the overlying strata to form local fractures and slabs on the upper continental slope (Laberg et al., 2013; Zhang et al., 2021). These slabs can then be softened, fractured and fragmented by high dip-angle fractures, ending up as a series of laterally spread blocks on a gentle submarine slope (Micallef et al., 2007; Baeten et al., 2014; Wu et al., 2021). Due to internal softening, deformation and sediment liquefaction, the size of these blocks often decreases with their transporting distance, before they are completely fragmented and liquefied into debrites and turbidity currents (Bull et al., 2009a; Alves, 2015; Cox et al., 2020).

RESULTS

Channels in MTCs with Differing Sinuosity Values

The northwestward transport of Storegga Slide has been recorded by seafloor grooves near the slide scar and intervals with discontinuous to chaotic seismic reflections (Haflidason et al., 2004) (Figs. 1a and 1d). Detailed bathymetric and structure maps reveal the northwest flank of the Storegga Slide (study area) as dipping to the southwest, with multiple small-scale failures post-dating the Storegga Slide and five distinct terraces delimited by scarps - terraces 1 to 5 and scarps S1 to S6 (Figs. 1b and 1d). Structural relief varies significantly on these terraces, from the smooth seafloor in Terrace 5 to the rugged ‘L’-shaped Terrace 1 undercutting through scarps S1 to S3 (Figs. 1b and 1c).

In this study area, MTC 1 is recognized in the lower continental slope to fills ooze evacuation structures (craters) below, perhaps as a result of focused fluid flow and sediment density reversal during Slide W (Riis et al., 2005; Lawrence and Cartwright, 2010; Omosanya et al., 2022). Above MTC 1, MTC 2 can be distinguished by its glide plane (Horizon H2) that eroded the top of MTC 1, where a group of NW-striking furrows is recorded in Terrace 2 with a sinuosity approaching 1.01 (Horizon H2; Figs. 1d, 2a, 3d, and 4). Towards the seafloor, a group of NW-striking grooves observed on both the relief and variance maps of Terrace 2 reveals a similar location and geometry to the glide-plane furrows below (Figs. 3a, 3d and 4). Seafloor grooves and underlying furrows have identical orientations and length, as well as the same location and geometry (Figs. 4c and 4d), representing the significant differential compaction within MTC 2.

Apart from these seafloor grooves representing glide plane furrows, discrete northwestward channels are recorded in MTC 2 by their differing variance and amplitude value on the seafloor, correlating to the transport of MTCs derived from the upper continental slope during the main Storegga Slide (Haflidason et al., 2004; 2005) (see Figs. 2c, 2d, 3b and 3c), These channels have an average sinuosity of 1.18 in Terrace 2, crossing the relatively straight grooves (Figs. 3b, 3c, 4c and 5). Beyond the 5km wide 'L'-shaped ramp, the channels in the southeast side upper slope reveal gently curved features with sinuosity about 1.02 (Figs. 2 and 5). The multiple grooves and sediment waves observed inside the turbidite channels differentiate them from debris channels, which contain chaotic strata with high variance coefficients (Fig. 2d).

MTCs with Slide Blocks

Due to the post-Storegga sediment drape is not voluminous and thick enough to cover failure-related features on the slope, the Storegga Slide scar and correlating MTCs are still exposed on the modern seafloor (Haflidason et al., 2004). Below the smooth seafloor of Terraces 4 and 5 (Fig. 6), two intervals with MTCs are identified as Units 1 and 2 (Figs. 7 and 8). Geochronological data indicate these MTCs, resulted from Slides S and R, can be respectively dated around 0.5 Ma and 0.3 Ma (Solheim et al., 2005) (Figs. 1d and 7). Despite the fact that these two slides encompass hundreds of square kilometres on the Norwegian margin, blocky features are only observed on the gentle north flank of the Storegga Slide, including our study area (Figs. 1 and 6).

In seismic data, slide blocks can be identified as a series of sub-parallel, coherent strata separated by chasms (Micallef et al., 2007) (Fig. 6). The development of these blocks on gentle slopes has been attributed to a reduction in lateral and toe support along with a propagation of glide planes through stratigraphic weak layers (Gauer et al., 2005; Kvalstad et al., 2005) (Fig. 7). These layer-parallel glide planes remove the support to overlying consolidated strata where internal friction angle could up to 20-30 degree, resulting in the generation of unstable slabs and subsequent fragmentation by steep (around 70-degree) fractures, forming laterally spread square-shaped blocks (Micallef et al., 2007; Wu et al., 2022).

Slide S Blocks in Terrace 4

Blocks in Slide S were translated above discrete glide planes identified at different stratigraphic levels (see 'shift point' in Fig. 7c). Above these glide planes, most blocks are curved on variance time slices (Fig. 6c). Blocks are 1000-2000 m apart and up to 80 ms tall (Fig. 7). Their length (L) varies from 800 m to 3600 m, while their width (W) ranges from 200 m to 600 m (Fig. 9). These slide blocks become larger downslope, where an eroded and irregular megablock is recognized (Figs. 6c and 7b). Moreover, a series of en echelon cracks are found to cut through Unit 1 on the back of the headwall scarp where the slide blocks originated from (Figs. 7b and 8a). The width of these cracks reaches only a few tens of meters, while their length ranges from 1 km to 5 km. Between these sub-parallel cracks and headwall scarps, incipient blocks and slabs are also identified (Fig. 8a).

Strata in Unit 2 comprise contourite deposits (Figs. 6a and 7c). Seismic reflections are continuous in chasms between Slide S blocks but folded and faulted above these same blocks (see the near-seafloor folds in Fig. 6a, and the faults above block 7 in Fig. 7b). Along the upper part of Terrace 4, these faults terminate at the glide planes of small-scale slumps formed near scarp S5 (Figs. 6b and 7b). On the lower part of Terrace 4, these same faults form scarps on the seafloor, such as the S4.1 – S4.4 above slide blocks 1 to 4 in Figs. 6b and

7c. Sourced from these scarps, the subsurface channels cross Scarp 4 and terraces 3 and 4, post-dating them after the main Storegga Slide (Figs. 1c, 6a-6b).

Slide R Blocks in Terrace 5

Slide R blocks are only observed in Terrace 5, occur in Unit 2, and are relatively small (see blocks on both sides of scarp S5 in Fig. 7b). Slide R blocks are closely spaced and up to 80 ms tall (Fig. 7a and 7b). Their length (L) varies from 800 m to 3600 m, with a width (W) from 200 m to 600 m (Figs. 8c, 8d and 9). Longitudinal blocks and chasms close to scarp S6 show a N-S strike, which is perpendicular to the local slope gradient (Fig. 8c). In contrast, blocks close to scarp S5 are more fragmented and strike to the NW (Fig. 8d). Behind scarp S5, a group of en echelon chasms is recognised between Slide R blocks (see 'chasms in Unit 2' in Fig. 8b). In contrast to other chasms, these en-echelon chasms are underlain by cracks developing in Unit 1, sharing a similar geometry, location, strike and length (see 'cracks in Unit 1' in Fig. 8a).

DISCUSSION

Sinuous Channels Formed by MTCs' Remobilization

In MTC 2, groups of channels present a sinuosity ranging from 1.02 in the southeast side upper slope to 1.18 in Terrace 2, where glide plane furrows are observed. These channels may record the transport direction of MTC 2, having developed together with its emplacement. However, the sinuous path they present in Terrace 2 does not correlate with the straight furrows observed on its glide plane, or the later slide complex would have been transported in multiple directions. Therefore, we interpret these sinuous channels to have developed after the onset of movement in MTC 2, during which the relatively straight furrows on its glide plane were able to erode MTC 1. Moreover, no marked changes of slope geometry, which could have increased the sinuosity of overlying flow, can be observed in MTC 2. This suggests that channels in Terrace 2 were as straight as those on the upper continental slope during their initial development.

The presence of undercut areas on the modern seafloor, and stratigraphic data from sediment cores, suggest a southwestward slope failure has partially evacuated MTC 2 through the 'L'-shaped ramp soon after the main Storegga Slide (Haflidason et al., 2005; Micallef et al., 2009) (Figs. 1b and 1c). Slope instability associated with this failure could not be limited to this 'L'-shaped ramp, as the failed MTC 2 is also observed in Terrace 2 (Figs. 2 and 4). The evacuation of MTCs through Terrace 1 (the lower section of 'L'-shaped ramp) also exposed the southwest scarp (S2) of Terrace 2 (Fig. 4). This enhanced the instability of MTC 2 in Terrace 2 by reducing its lateral support, and thus contributing to its remobilization.

Together with the coexistence of straight channels on southeast side upper continental slope (Fig. 2) and straight glide-plane furrows in Terrace 2 (Fig. 3d), the sinuous channels in Terrace 2 are here related to the remobilization of MTC 2 after its lateral support was removed. This remobilization did not evacuate the entire MTC 2 from Terrace 2 but was enough to deform MTC 2 internally, increasing the sinuosity of pre-existing channels. The development of MTC 2 and accompanying channels followed the sequence of events below:

1) MTC 2 was first mobilized during the initial NW transport of Storegga Slide and later deposited along the northwest flank with low-sinuosity internal channels and glide-plane furrows (Figs. 2, 3d, 4d and 10a).

2) Soon after, a southwestward slope failure sourced from the northwest flank undercut MTC 2 through a 'L'-shaped ramp, exposing Scarp S2 on the seafloor (Figs. 1b and

3a). Due to insufficient lateral support near Terrace 2, the still unconsolidated MTC 2 was remobilized and began to move over the evacuated ramp, deforming the internal channels previously formed (Figs. 3b, 3c, 4c and 10b).

3) Since then, differential compaction has followed the trace of glide-plane furrows at the base of MTC 2, forming grooves on the modern seafloor that cross the sinuous channels formed during the remobilization in the previous stage (Fig. 4c and 10c).

Effect of MTCs' Reactivation on Post-failure Strata

The Reactivated MTCs (Slide S) Impacts the Development of Slide R

Slide R comprises laterally spread blocks has been thought to remain stable since they were formed, as no fractures or seafloor cracks can be observed within the overlying strata. However, the chasms between Slide R blocks (Fig. 8b) and the underlying cracks in Unit 1 (Fig. 8a), with matching geometries to the chasms, indicate a later episode of local extension.

The layer-parallel glide planes and overlying square-shaped blocks suggest that the development of Slide S was accompanied by the propagation of its glide plane upslope, resulting in a series of extensional cracks in Unit 1 (Figs. 7b and 8a). While the chasms preserved between Slide R blocks appear to be controlled by the underlying cracks in Slide S, it is possible that cracks associated with Slide S propagated into Unit 2 as longitudinal chasms during Slide R movement (see the red dashed line in Figs. 8a and 8b). In addition, the reactivation of Slide S is attributed to the evacuation of Slide S blocks and subsequent reduction in lateral support (Bull et al., 2009b). Therefore, our seismic interpretation suggest that a reactivated Slide S was able to induce the movement of Slide R blocks by reducing lateral support on the slope via the propagation of their glide plane and by forming extensional cracks, thus fracturing the overlying MTC. Although the cracks are narrow, the reactivation of the Slide S could be subtle on the upper slope, without significant sediment transport.

Seafloor Scarps and Slumps Indicate Long-term Instability of MTCs

In Terrace 4, there are two intervals above a basal glide plane, with laterally spread Slide S blocks and overlying contourites. Small-scale folds above these blocks (Figs. 6a and 7a), channels near scarps S4.1-S4.4, and slumps near S5 (Figs. 6b, 7b and 7c), are features indicating an unstable Terrace 4. Differential compaction within contourite deposits, resulting in small folds above blocks, may be responsible for this instability. However, the Storegga Slide scar and correlating MTCs are exposed on the modern seafloor (Haflidason et al., 2004), suggesting the post-slide deposition is inconspicuous to enhance a differential compaction and trigger this slope instability.

In parallel, slope undercutting during the main Storegga Slide could have also increased the instability of Terrace 4 by reducing lateral support along Scarp S4. Faults are observed below the seafloor MTCs in the lower and upper parts of Terrace 4 (Figs. 7b and 7c), while continuous reflections in the middle of the terrace suggest a relatively stable contourites interval (Figs. 7a and 7b). Due to these faults and overlying seafloor slope failures are only located above Slide S blocks (Figs. 7b and 7c), we suggest that these laterally spread blocks should have been reactivated during the emplacement of Storegga Slide and led to local slope failure above.

A Model Explaining the Development of Unstable MTCs with Laterally Spread Blocks

Previous studies have suggested that the strike of laterally spread blocks (also named as ‘spreading blocks’) can be parallel to slide headwalls and perpendicular to their direction of downslope transport when formed in a retrogressive sequence (Kvalstad et al., 2005; Baeten et al., 2014).These retrogressively spread blocks are fragmented downslope, where they decrease in size via strain softening and intermixing of flows during their downslope transport (Bull et al., 2009a; Cox et al., 2020). Conversely, newly formed (or incipient) slide blocks can be identified on the upper continental slope as intact features with relatively larger sizes due to their limited movement (Micallef et al., 2007). Given that fragmented and rotated blocks are observed on the lower part of Terrace 5 (Figs. 8b, 8c and 8d), the spreading of Slide R blocks can be related to a retrogressive sequence (Bull et al., 2009b), similarly to blocks observed in Slide S, Slide R and within the Storegga Slide.

Contrasting with the Slide R blocks in Terrace 5, Slide S blocks in Terrace 4 are larger towards the lower continental slope (Figs. 6c, 7 and 9). As block size cannot increase during their downslope transport, rather decreasing by strain softening and fragmentation, the large blocks observed in the lower part of Terrace 4 suggest they were remarkably large when first formed. While the smaller blocks, such as block 7 in Figs. 6c and 7b, along the headwall of Terrace 4, hint at a smaller initial size. As the size of laterally spread blocks on gentle slopes is determined by the physical properties of the failed strata, abrupt lithological changes are expected to have significantly changed the strength of Unit 1 as well as the size of Slide S blocks along Terrace 4 (Puzrin et al., 2017) (Fig. 6c). However, the similar height of blocks and dip angles of their bounding fractures suggest a relatively homogeneous strength in the strata composing Unit 1 (Micallef et al., 2007; Wu et al., 2021). Hence, the smaller blocks in the upper part of Terrace 4 may not represent their initial size, but result from later fragmentation after their initial development.

Following slope undercutting, glide plane propagation in an upslope direction can induce the lateral spreading of slide blocks, as observed in Slide R and the Storegga Slide per se (Micallef et al., 2007a; Solheim et al., 2005). Such a glide plane can propagate much beyond a slide's headwall to fragment the overlying strata into slabs, as those observed in Unit 1 (Baeten et al., 2014; Zhang et al., 2021) (Figs. 7b and 8a). Failed slabs are large and irregular, but maintaining a coherent inner structure until they are fragmented into series of blocks during their downslope transport (Micallef et al., 2007; Dey et al., 2016). Numerical simulations further suggest that, during the fragmentation of moving slabs, blocks can spread from both its lower and upper boundaries (Debnath, 2018; Zhang et al., 2021).

Laterally spread blocks generated from the lower boundary of a slab may also form retrogressively as they use a fully evacuated lower slope to accommodate their movement (Alves, 2015; Zhang et al., 2021) (see the 'retrogressive model' in Fig. 10d). Laterally spread blocks detached from the upper boundary of a slab develop progressively and are partially supported by the moving slab, limiting their transport (Dong et al., 2017; Debnath, 2018; Zhang et al., 2021) (see the 'progressive model' in Fig. 10e). Hence, sliding slabs are transient features before being fully fragmented into series of retrogressively and progressively spread blocks on the lower and upper parts of submarine slopes, respectively (Dong et al., 2017; Debnath, 2018). Together with the extensional cracks and smaller blocks along the headwall of Slide S (Scarp 5 in Figs. 6c and 8a), the large and irregular block close to scarp S4 could have formed one of the failed slabs, while the other blocks in Terrace 4 could be progressively spread from moving slabs, in an event comprising, at least, two stages:

1) The north flank of the Storegga area was undercut by Slide S and a glide plane propagated towards the upper slope at the same time. On the lower slope, blocks were laterally spread from evacuated scarps in a retrogressive sequence, showing a reduction in size with transporting distance and rotation (blocks in Fig. 10d). On the upper slope, the propagation of glide plane eventually breakup overlying strata, resulting in extensional cracks and incipient slabs (cracks and slabs in Figs. 8a and 10d). Similar features are identified on the north flank and headwall region of Storegga Slide (Solheim et al., 2005).

2) Together with the downslope transport of slabs and retrogressively spread blocks from their lower scarps, blocks were also progressively spread from their upper scarps at the same time, generating new and large Slide S blocks in the lower part of Terrace 4 (Figs. 6c, 7 and 10e). These progressive blocks were supported by slabs from the lower slope, thus preventing further transportation and maintaining their instability until slope undercutting removes this lateral support.

Slope Undercutting As a Trigger of Blocky MTCs' Reactivation

A distinct feature of Slide S is the presence of larger blocks towards the lower continental slope (Fig. 6c). Indicated by the cracks and incipient slabs on the upper slope (Fig. 8a), these blocks are likely formed from the fragmentation of slabs and progressively spread blocks (Fig. 10e). In contrast to retrogressively spread blocks, which have an evacuated lower slope (Alves, 2015; Zhang et al., 2021), these progressive blocks are laterally supported by slabs until they are fully fragmented (Dong et al., 2017; Debnath, 2018). However, accompanied by the formation of cracks in Terrace 5 and slope failures in Terrace 4, recurrent reactivation of Slide S is perhaps related to the undercutting of the lower continental slope. This removal of lower slope support could have triggered the long-term instability of the progressively spread blocks. In comparison, retrogressively spread blocks may not have been reactivated due to the pre-existing evacuation of their lower slope.

Another important aspect concerns the lithification of Slide S blocks prior to their initial development, which led to more consolidated material in Slide S than in the contourites that drape it. This greater consolidation contrasts with the reduced shear strength of the underlying marine clay that forms Slide S glide plane. Consequently, Slide S blocks are the most consolidated features of Units 1 and 2 in Terrace 4, hindering the development of low-angle extensional fractures. Instead, they led to the formation of high-angle faults during block reactivation, as observed near the exposed scarps S4.1-S4.4 (Figs. 6b, 7c, and 10f).

IMPLICATIONS

The instability of continental slopes has been assessed in previous work, which gave greater focus to pre-instability scenarios (Leynaud et al., 2009; Urlaub and Hjelstuen, 2020). Monitoring seafloor deformation preceding slope failure requires multiple approaches, such as the use of multibeam, geophysical and geodetic data (Maksymowicz et al., 2017; Urlaub et al., 2018). Based on the mapping of geomorphological features from high-resolution 3D seismic data, this work recognizes the presence of channels, seafloor failure scars and cracks as materializing the reactivation of MTCs near the Storegga Slide. These observations provide evidence for post-slide instability where emplaced MTCs remain unstable well after their failure. These MTCs become the subject of instability, being reactivated to trigger further instability features. Although this kind of seafloor deformation occurs locally near the larger Storegga area, its potential to repeatedly remobilize near-seafloor strata must not be ignored. Considering the wide distribution of MTCs along continental margins, such as the Norwegian margin, Mediterranean Sea, West Africa, South China Sea and east USA (Solheim et al., 2005a; Chaytor et al., 2007; Dalla Valle et al., 2015; Li et al., 2017; Sun et al., 2018b), a re-evaluation of MTCs-driven slope instability is essential to protect submarine infrastructure and coastal populations.

CONCLUSIONS

This study identifies key features marking the post-depositional reactivation of mass transport complexes (MTCs) and shows them to be underestimated marine geohazards on the Norwegian margin. Long-term slope instability was promoted by the presence of underconsolidated MTCs and laterally spread blocks. Key conclusions of this work can be summarized as follows:

a) The remobilization of unconsolidated MTCs can be recorded by the increased sinuosity of channels that developed during the initial transport of MTCs from upper continental slope.

b) Reactivated MTCs with laterally spread blocks can cause seafloor fractures and scarps, accompanied by slumps and channels crossing the slide scar.

c) Indicated by the cracks and incipient slabs on the upper continental slope and larger blocks on the lower slope, blocks are suggested to be progressively spread from moving slabs, leaving unstable MTCs with supports from lower slope.

d) The instability of MTCs may be maintained for millions of years, and is most frequently triggered by slope undercutting, making them hitherto underestimated geohazards.

As a consequence, this study demonstrates that pre-existing MTCs can be a significant preconditioning factor for long-term slope instability on continental slopes. Slope undercutting develops self-sustaining areas with recurrent slope failure, as that documented in this work on the northwest flank of the Storegga Slide.

ACKNOWLEDGMENTS

The authors would like to acknowledge the permission conceded by NTNU-NPD-Schlumberger Petrel Ready Database for the use of the Seismic and wellbore data presented in this paper. Schlumberger (provider of Petrel®) is acknowledged for the provision of the academic licenses to Cardiff University's 3D seismic Lab. This research did not receive any specific grants from funding agencies in the public, commercial, or not-for-profit sectors. Dr. Wei Li is specially funded by CAS Pioneer Hundred Talents Program. We thank Editor Mihai Ducea, Associate Editor Stefano Mazzoli, reviewer Gian Andrea Pini and another anonymous reviewer for their constructive comments.

The seismic data (Survey MC3DMGS2002, acquired in 2002 by PGS) that support the findings are available from the Norwegian University of Science and Technology (NTNU) or DISKOS. Restrictions apply to the availability of these data, which were used under license for this study. Data are available with permission of NTNU. For access to the data through NTNU, contact: Knut Back < knut.reitan.backe@ntnu.no >.

REFERENCES CITED

Alves, T.M., 2010, 3D Seismic examples of differential compaction in mass-transport deposits and their effect on post-failure strata: Marine Geology, v. 271, p. 212–224, doi:10.1016/j.margeo.2010.02.014.

Alves, T.M., 2015, Submarine slide blocks and associated soft-sediment deformation in deep-water basins: A review: Marine and Petroleum Geology, v. 67, p. 262–285, doi:10.1016/j.marpetgeo.2015.05.010.

Alves, T.M., Cardona, S., and Rodrigues, M.C.N.L., 2022, Mass transport processes, injectites and styles of sediment remobilization: Deepwater Sedimentary Systems: Science, Discovery, and Applications, p. 361–406, doi:10.1016/B978-0-323-91918-0.00013-X.

Alves, T.M., Kurtev, K., Moore, G.F., and Strasser, M., 2014, Assessing the internal character, reservoirpotential,and seal competence of mass-transport deposits using seismic texture: A geophysical and petrophysical approach: AAPG Bulletin, v. 98, p. 793–824, doi:10.1306/09121313117.

Baeten, N.J., Laberg, J.S., Vanneste, M., Forsberg, C.F., Kvalstad, T.J., Forwick, M., Vorren, T.O., and Haflidason, H., 2014, Origin of shallow submarine mass movements and their glide planes-Sedimentological and geotechnical analyses from the continental slope off northern Norway: Journal of Geophysical Research: Earth Surface, v. 119, p. 2335–2360, doi:10.1002/2013JF003068.

Berg, K., Solheim, A., and Bryn, P., 2005, The Pleistocene to recent geological development of the Ormen Lange area: Marine and Petroleum Geology, v. 22, p. 45–56, doi:10.1016/j.marpetgeo.2004.10.009.

Bryn, P., Solheim, A., Berg, K., Lien, R., Forsberg, C.F., Haflidason, H., Ottesen, D., and Rise, L., 2003, The Storegga Slide Complex; Repeated Large Scale Sliding in Response to Climatic Cyclicity, *in* p. 215–222, doi:10.1007/978-94-010-0093-2_24.

Bugge, T., Belderson, R.H., and Kenyon, N.H., 1988, The Storegga slide: Philosophical Transactions - Royal Society, Series A, v. 325, p. 357–388, doi:10.1098/rsta.1988.0055.

Bull, S., Cartwright, J., and Huuse, M., 2009a, A review of kinematic indicators from mass-transport complexes using 3D seismic data: Marine and Petroleum Geology, v. 26, p. 1132–1151, doi:10.1016/j.marpetgeo.2008.09.011.

Bull, S., Cartwright, J., and Huuse, M., 2009b, A subsurface evacuation model for submarine slope failure: Basin Research, v. 21, p. 433–443, doi:10.1111/j.1365-2117.2008.00390.x.

Camerlenghi, A., and Pini, G.A., 2009, Mud volcanoes, olistostromes and Argille scagliose in the Mediterranean region: Sedimentology, v. 56, p. 319–365, doi:10.1111/j.1365-3091.2008.01016.x.

Chaytor, J.D., Twichell, D.C., Brink, U.S. Ten, Buczkowski, B.J., and Andrews, B.D., 2007, Revisiting Submarine Mass Movements Along The U.S. Atlantic Continental Margin: Implications For Tsunami Hazards, *in* Submarine Mass Movements and Their Consequences, Dordrecht, Springer Netherlands, p. 395–403, doi:10.1007/978-1-4020-6512-5_41.

Conti, S., Fontana, D., Lucente, C.C., and Pini, G.A., 2014, Relationships between seep-carbonates, mud volcanism and basin geometry in the Late Miocene of the northern Apennines of Italy: The Montardone mélange: International Journal of Earth Sciences, v. 103, p. 281–295, doi:10.1007/s00531-013-0928-y.

Cox, D.R., Huuse, M., Newton, A.M.W., Gannon, P., and Clayburn, J., 2020, Slip sliding away: Enigma of large sandy blocks within a gas-bearing mass transport deposit, offshore northwestern Greenland: AAPG Bulletin, v. 104, p. 1011–1043, doi:10.1306/10031919011.

Dalla Valle, G., Gamberi, F., Foglini, F., and Trincardi, F., 2015, The Gondola Slide: A mass transport complex controlled by margin topography (South-Western Adriatic Margin, Mediterranean Sea): Marine Geology, v. 366, p. 97–113, doi:10.1016/j.margeo.2015.05.001.

Dalland, A., 1988, A lithostratigraphic scheme for the Mesozoic and Cenozoic succesion offshore Norway north of 62° N: Norw. Petrol. Dir. Bull.,.

Debnath, B., 2018, Modelling of downslope displacement of failed soil blocks originating from submarine landslides:, http://research.library.mun.ca/id/eprint/13399.

Dellisanti, F., Pini, G.A., Tateo, F., and Baudin, F., 2008, The role of tectonic shear strain on the illitization mechanism of mixed-layers illite-smectite. A case study from a fault zone in the Northern Apennines, Italy: International Journal of Earth Sciences, v. 97, p. 601–616, doi:10.1007/s00531-007-0180-4.

Dey, R., Hawlader, B.C., Phillips, R., and Soga, K., 2016, Numerical modelling of submarine landslides with sensitive clay layers: Geotechnique, v. 66, p. 454–468, doi:10.1680/jgeot.15.P.111.

Dong, Y., Wang, D., and Randolph, M.F., 2017, Runout of Submarine Landslide Simulated with Material Point Method: Procedia Engineering, v. 175, p. 357–364, doi:10.1016/j.proeng.2017.01.045.

Gatter, R., Clare, M.A., Kuhlmann, J., and Huhn, K., 2021, Characterisation of weak layers, physical controls on their global distribution and their role in submarine landslide formation: Earth-Science Reviews, v. 223, p. 103845, doi:10.1016/j.earscirev.2021.103845.

Gauer, P., Kvalstad, T.J., Forsberg, C.F., Bryn, P., and Berg, K., 2005, The last phase of the Storegga Slide: Simulation of retrogressive slide dynamics and comparison with slide-scar morphology: Marine and Petroleum Geology, v. 22, p. 171–178, doi:10.1016/j.marpetgeo.2004.10.004.

GEBCO Bathymetric Compilation Group 2020, 2020, GEBCO_2020 Grid:, doi:10.5285/a29c5465-b138-234d-e053-6c86abc040b9.

Giona Bucci, M., Micallef, A., Urlaub, M., Mountjoy, J., and Barrett, R., 2022, A global review of subaqueous spreading and its morphological and sedimentological characteristics: A database for highlighting the current state of the art: Geomorphology, v. 414, p. 108397, doi:10.1016/j.geomorph.2022.108397.

Haflidason, H., Lien, R., Sejrup, H.P., Forsberg, C.F., and Bryn, P., 2005, The dating and morphometry of the Storegga Slide: Marine and Petroleum Geology, v. 22, p. 123–136, doi:10.1016/j.marpetgeo.2004.10.008.

Haflidason, H., Sejrup, H.P., Nygård, A., Mienert, J., Bryn, P., Lien, R., Forsberg, C.F., Berg, K., and Masson, D., 2004, The Storegga Slide: Architecture, geometry and slide development: Marine Geology, v. 213, p. 201–234, doi:10.1016/j.margeo.2004.10.007.

Harbitz, C.B., Løvholt, F., Pedersen, G., and Masson, D.G., 2006, Mechanisms of tsunami generation by submarine landslides: A short review: Norsk Geologisk Tidsskrift, v. 86, p. 255–264.

Jing, S., Alves, T., and Omosanya, K.O., 2022, Styles of slope instability on a Quaternary sub-arctic continental margin: The northwest flank of the Storegga Slide: Marine Geology, v. 454, p. 106933, doi:10.1016/j.margeo.2022.106933.

Jing, S., Alves, T.M., Omosanya, K.O., Hales, T.C., and Ze, T., 2020, Tectonic evolution of strike-slip zones on continental margins and their impact on the development of submarine landslides (Storegga Slide, northeast Atlantic): Bulletin of the Geological Society of America, v. 132, p. 2397–2414, doi:10.1130/B35421.1.

Kvalstad, T.J., Andresen, L., Forsberg, C.F., Berg, K., Bryn, P., and Wangen, M., 2005, The Storegga slide: Evaluation of triggering sources and slide mechanics: Marine and Petroleum Geology, v. 22, p. 245–256, doi:10.1016/j.marpetgeo.2004.10.019.

L'Heureux, J.-S. et al., 2012, Identification of Weak Layers and Their Role for the Stability of Slopes at Finneidfjord, Northern Norway, *in* Submarine Mass Movements and Their Consequences, Dordrecht, Springer Netherlands, p. 321–330, doi:10.1007/978-94-007-2162-3_29.

Laberg, J.S., Baeten, N.J., Lågstad, P., Forwick, M., and Vorren, T.O., 2013, Formation of a large submarine crack during the final stage of retrogressive mass wasting on the continental slope offshore northern Norway: Marine Geology, v. 346, p. 73–78, doi:10.1016/j.margeo.2013.08.008.

Lawrence, G.W.M., and Cartwright, J.A., 2010, The stratigraphic and geographic distribution of giant craters and remobilised sediment mounds on the mid Norway margin, and their relation to long term fluid flow: Marine and Petroleum Geology, v. 27, p. 733–747, doi:10.1016/j.marpetgeo.2009.10.012.

Lewis, K.B., Collot, J.Y., and Lallemand, S.E., 1998, The dammed Hikurangi Trough: A channel-fed trench blocked by subducting seamounts and their wake avalanches (New Zealand-France GeodyNZ Project): Basin Research, v. 10, p. 441–468, doi:10.1046/j.1365-2117.1998.00080.x.

Leynaud, D., Mienert, J., and Vanneste, M., 2009, Submarine mass movements on glaciated and non-glaciated European continental margins: A review of triggering mechanisms and preconditions to failure: Marine and Petroleum Geology, v. 26, p. 618–632, doi:10.1016/j.marpetgeo.2008.02.008.

Li, W. et al., 2017, Morphology, age and sediment dynamics of the upper headwall of the Sahara Slide Complex, Northwest Africa: Evidence for a large Late Holocene failure: Marine Geology, v. 393, p. 109–123, doi:10.1016/j.margeo.2016.11.013.

Locat, J., Leroueil, S., Locat, A., and Lee, H., 2016, Weak layers: Their definition and classification from a geotechnical perspective, *in* Submarine Mass Movements and Their Consequences, 6th International Symposium, Springer, p. 3–12, doi:10.1007/978-3-319-00972-8_1.

Maksymowicz, A., Chadwell, C.D., Ruiz, J., Tréhu, A.M., and Weinrebe, W., 2017, Coseismic seafloor deformation in the trench region during the Mw8 . 8 Maule megathrust earthquake: , p. 1–8, doi:10.1038/srep45918.

Masson, D.G., Harbitz, C.B., Wynn, R.B., Pedersen, G., and Løvholt, F., 2006, Submarine landslides: Processes, triggers and hazard prediction: Philosophical Transactions of the Royal Society A: Mathematical, Physical and Engineering Sciences, v. 364, p. 2009–2039, doi:10.1098/rsta.2006.1810.

Mesri, G., and Huvaj-Sarihan, N., 2012, Residual Shear Strength Measured by Laboratory Tests and Mobilized in Landslides: Journal of Geotechnical and Geoenvironmental Engineering, v. 138, p. 585–593, doi:10.1061/(asce)gt.1943-5606.0000624.

Micallef, A., Masson, D.G., Berndt, C., and Stow, D.A.V., 2009, Development and mass movement processes of the north-eastern Storegga Slide: Quaternary Science Reviews, v. 28, p. 433–448, doi:10.1016/j.quascirev.2008.09.026.

Micallef, A., Masson, D.G., Berndt, C., and Stow, D.A.V., 2007, Morphology and mechanics of submarine spreading: A case study from the Storegga Slide: Journal of Geophysical Research: Earth Surface, v. 112, p. 1–21, doi:10.1029/2006JF000739.

Mienert, J., Vanneste, M., Haflidason, H., and Bünz, S., 2010, Norwegian margin outer shelf cracking: A consequence of climate-induced gas hydrate dissociation? International Journal of Earth Sciences, v. 99, p. 207–225, doi:10.1007/s00531-010-0536-z.

Moscardelli, L., and Wood, L., 2016, Morphometry of mass-transport deposits as a predictive tool: Bulletin of the Geological Society of America, v. 128, p. 47–80, doi:10.1130/B31221.1.

Nugraha, H.D., Jackson, C.A.-L., Johnson, H.D., Hodgson, D.M., and Clare, M.A., 2022, Extreme erosion by submarine slides: Geology, v. XX, p. 1–5, doi:10.1130/g50164.1.

Ogata, K., Festa, A., Pini, G.A., and Alonso, J.L., 2019a, Submarine Landslide Deposits in Orogenic Belts: , p. 1–26, doi:10.1002/9781119500513.ch1.

Ogata, K., Festa, A., Pini, G.A., Pogačnik, and Lucente, C.C., 2019b, Substrate deformation and incorporation in sedimentary mélanges (olistostromes): Examples from the northern Apennines (Italy) and northwestern Dinarides (Slovenia): Gondwana Research, v. 74, p. 101–125, doi:10.1016/j.gr.2019.03.001.

Ogata, K., Mountjoy, J.J., Pini, G.A., Festa, A., and Tinterri, R., 2014, Shear zone liquefaction in mass transport deposit emplacement: A multi-scale integration of seismic reflection and outcrop data: Marine Geology, v. 356, p. 50–64, doi:10.1016/j.margeo.2014.05.001.

Omosanya, K.O., 2018, Episodic fluid flow as a trigger for Miocene-Pliocene slope instability on the Utgard High, Norwegian Sea: Basin Research, v. 30, p. 942–964, doi:10.1111/bre.12288.

Omosanya, K.O., Duffaut, K., Alves, T.M., Eruteya, O.E., Johansen, S.E., and Waldmann, N., 2022, Giant paleo-seafloor craters and mass wasting associated with magma-induced uplift of the upper crust: Scientific Reports, v. 12, p. 4392, doi:10.1038/s41598-022-08205-0.

Pickering, K.T., and Hiscott, R.N., 2015, Deep marine systems: processes, deposits, environments, tectonics and sedimentation: John Wiley & Sons.

Pini, G.A., Ogata, K., Camerlenghi, A., Festa, A., Lucente, C.C., and Codegone, G., 2012, Sedimentary mélanges and fossil mass- Transport complexes: A key for better understanding submarine mass movements? Submarine Mass Movements and Their Consequences - 5th International Symposium, p. 585–594, doi:10.1007/978-94-007-2162-3_52.

Puzrin, A.M., Gray, T.E., and Hill, A.J., 2017, Retrogressive shear band propagation and spreading failure criteria for submarine landslides: Geotechnique, v. 67, p. 95–105, doi:10.1680/jgeot.15.P.078.

Reiche, S., Hjelstuen, B.O., and Haflidason, H., 2011, High-resolution seismic stratigraphy, sedimentary processes and the origin of seabed cracks and pockmarks at Nyegga, mid-Norwegian margin: Marine Geology, v. 284, p. 28–39, doi:10.1016/j.margeo.2011.03.006.

Riis, F., Berg, K., Cartwright, J., Eidvin, T., and Hansch, K., 2005, Formation of large, crater-like evacuation structures in ooze sediments in the Norwegian Sea. Possible implications for the development of the Storegga Slide: Marine and Petroleum Geology, v. 22, p. 257–273, doi:10.1016/j.marpetgeo.2004.10.023.

Sawyer, D.E., Flemings, P.B., Dugan, B., and Germaine, J.T., 2009, Retrogressive failures recorded in mass transport deposits in the Ursa Basin, Northern Gulf of Mexico: Journal of Geophysical Research: Solid Earth, v. 114, p. 1–20, doi:10.1029/2008JB006159.

Shanmugam, G., 2021, Deep-Water Processes and Deposits: 965–1009 p., doi:10.1016/b978-0-12-409548-9.12541-2.

Solheim, A., Berg, K., Forsberg, C.F., and Bryn, P., 2005a, The Storegga Slide complex: Repetitive large scale sliding with similar cause and development: Marine and Petroleum Geology, v. 22, p. 97–107, doi:10.1016/j.marpetgeo.2004.10.013.

Solheim, A., Bryn, P., Sejrup, H.P., Mienert, J., and Berg, K., 2005b, Ormen Lange - An integrated study for the safe development of a deep-water gas field within the Storegga Slide Complex, NE Atlantic continental margin; executive summary: Marine and Petroleum Geology, v. 22, p. 1–9, doi:10.1016/j.marpetgeo.2004.10.001.

Sun, Q., Alves, T.M., Lu, X., Chen, C., and Xie, X., 2018a, True Volumes of Slope Failure Estimated From a Quaternary Mass-Transport Deposit in the Northern South China Sea: Geophysical Research Letters, v. 45, p. 2642–2651, doi:10.1002/2017GL076484.

Sun, Q., Cartwright, J., Xie, X., Lu, X., Yuan, S., and Chen, C., 2018b, Reconstruction of repeated Quaternary slope failures in the northern South China Sea: Marine Geology, v. 401, p. 17–35, doi:10.1016/j.margeo.2018.04.009.

Talling, P.J. et al., 2007, Onset of submarine debris flow deposition far from original giant landslide: Nature, v. 450, p. 541–544, doi:10.1038/nature06313.

Urgeles, R., and Camerlenghi, A., 2013, Submarine landslides of the Mediterranean Sea: Trigger mechanisms, dynamics, and frequency-magnitude distribution: Journal of Geophysical Research: Earth Surface, v. 118, p. 2600–2618, doi:10.1002/2013JF002720.

Urlaub, M., and Hjelstuen, B.O., 2020, A numerical investigation of excess pore pressures and continental slope stability in response to ice-sheet dynamics: Geological Society Special Publication, v. 500, p. 255–266, doi:10.1144/SP500-2019-185.

Urlaub, M., Petersen, F., Gross, F., Bonforte, A., Puglisi, G., Guglielmino, F., Krastel, S., Lange, D., and Kopp, H., 2018, Gravitational collapse of Mount Etna's southeastern flank: Science Advances, v. 4, p. 1–8, doi:10.1126/sciadv.aat9700.

Wang, X., Wang, Y., He, M., Chen, W., Zhuo, H., Gao, S., Wang, M., and Zhou, J., 2017, Genesis and evolution of the mass transport deposits in the middle segment of the Pearl River canyon, South China Sea: Insights from 3D seismic data: Marine and Petroleum Geology, v. 88, p. 555–574, doi:10.1016/j.marpetgeo.2017.08.036.

Wu, N., Jackson, C.A.-L., Clare, M.A., Hodgson, D., Nugraha, H.D., Steventon, M., and Zhong, F.G., 2022, Diagenetic priming of submarine landslides in ooze-rich substrates:, doi:https://doi.org/10.31223/X50P9Q.

Wu, N., Jackson, C.A.L., Johnson, H.D., Hodgson, D.M., Clare, M.A., Nugraha, H.D., and Li, W., 2021, The formation and implications of giant blocks and fluid escape structures in submarine lateral spreads: Basin Research, v. 33, p. 1711–1730, doi:10.1111/bre.12532.

Zhang, W., Klein, B., Randolph, M.F., and Puzrin, A.M., 2021, Upslope Failure Mechanisms and Criteria in Submarine Landslides: Shear Band Propagation, Slab Failure and Retrogression: Journal of Geophysical Research: Solid Earth, v. 126, p. 1–29, doi:10.1029/2021JB022041.

FIGURE CAPTIONS

Figure 1. **a**) Location of study area on the northwest flank of the Storegga Slide, mid-Norwegian margin, highlighting the distribution of the Storegga Slide complex (Solheim et al., 2005a) and seafloor cracks (Mienert et al., 2010; Reiche et al., 2011). Map is modified from GEBCO Bathymetric Compilation Group (2020). The gray-shaded area represents the location of south Modgunn Arch. **b**) Detailed two-way time (twt) map of the seafloor, as extracted from seismic data. The seismic profiles and key areas discussed in this work are highlighted by the black lines and rectangles. **c)** Relationship amongst the Storegga Slide complex covering the variance map of basal glide plane (H3) in study area, including slides W, S, R, and the Storegga Slide (Solheim et al., 2005a). **d**) Seismic profile crossing all the slope terraces in the study area with schematic slide stratigraphy in the Naust Formation (Naust Fm.). Location is shown in Figs. 1b and 1c. Horizon H1: seafloor; Horizon H2: inner glide plane between MTCs 1 and 2; Horizon H3: basal glide plane of the Storegga Slide complex; Horizon H4: top of Kai Formation; Horizon H5: top of Brygge Formation; Horizon H6: base of the post-breakup units, remaining intact during the Storegga Slide complex. S1-S6: slope scarps separating terraces.

Figure 2. **a**) Seismic profile showing typical turbidite and debris channels on the southeast side upper continental slope. The location of the profile is shown in Figs. 1b and 2b-2d. MTC 1 was deposited in association with Slide W, before the Storegga Slide proper (Bryn et al., 2003; Omosanya et al., 2022). **b**) TWT map of the seafloor (Horizon H1). The grooves and sediment waves inside the turbidite channels distinguish them from debris channels, the latter of which present a rugged internal character. Location of the TWT map is shown in Figs. 1b and 1c. **c**) RMS amplitude map of the seafloor (H1). The chaotic facies of strata inside debris channels contrasts with that of turbidite channels, which are smoother and show lineations in

them. **d**) Variance map of the seafloor (Horizon H1). The chaotic and high variance of debris channels are indicative of their presence on the seafloor.

Figure 3. **a**) TWT map of the seafloor (Horizon H1). A group of NW-SE grooves is observed on the seafloor and marked by a white dashed line. **b-c**) RMS amplitude and Variance maps of the seafloor (H1). Submarine channels are shown as linear features with higher RMS amplitude and variance values. **d**) TWT map of the inner glide plane (Horizon H2) between MTCs 1 and 2 in Fig. 4. A group of glide-plane furrows is marked by black dashed lines. The detail of grooves and furrows can be observed in Fig. 4. The location of the maps is shown in Figs. 1b and 1c.

Figure 4. **a-b**) Seismic profile crossing Terrace 2. Seafloor grooves are marked by black circles, and the glide plane furrows are highlighted by rectangles. The location of the seismic profile is shown in Fig. 3d; **c**) and **d**) Relief maps of the seafloor (horizon H1) and the glide plane of MTC 2 (horizon H2). The distribution of grooves and furrows are documented as local depressions on the seafloor and glide plane, sharing the same location and geometry. The channels shown in Figs. 3b and 3c can also be observed in c) as linear depressions.

Figure 5. Sinuosity of channels and furrows in study area. The channels on southeast side upper continental slope and glide-plane furrows reveal a very low sinuosity between 1.01 and 1.02, whereas the channels in Terrace 2 show an average sinuosity of 1.18.

Figure 6. **a-b)** TWT and variance maps of the seafloor (Horizon H1). The location of the maps is shown in Figs. 1b and 1c. Multiple local folds contributed to the formation of a rugged Terrace 4. Channels (C*) and slumps are sourced from seafloor scarps crossing scarp

S4 and Terraces 3 and 4. **c)** Variance-slice 50 ms above the basal glide plane (Horizon H3) of laterally spread blocks. In Terrace 4, the size of Slide S blocks increases towards lower slope.

Figure 7. **a-c**) Selected seismic profiles across Terrace 4. The locations of the profiles are shown in Fig. 6. Slide blocks in Units 1 and 2 are separated by scarp S5. Slide S blocks are located on the lower continental slope (Unit 1) and were draped by a thin interval of contourites. Seismic reflections in these contourites are continuous in the chasms but folded and faulted above discrete slide blocks. The 'eroded block' in b) corresponds to the irregular block in Fig. 6c, forming the largest block in Terrace 4. The seafloor scarps S4.1-S4.4 in Fig. 6b relate to underlying Slide S blocks 1-4 in c). Discrete glide plane below Slide S blocks shift stratigraphic levels in c). Slide R blocks are located in Terrace 5 and are underlain by incipient Slide S blocks and cracks.

Figure 8. **a)** Variance maps of the basal glide plane of Slide R blocks (Horizon H3). A group of extensional cracks are located in Unit 1 on the northeast side upper continental slope, as observed in Fig. 7b. **b)** Variance map of a time-slice 50 ms above the basal glide plane of Slide R blocks (Horizon H3-50ms). Cracks in Unit 1 can be recognized as longitudinal chasms in the overlying Unit 2. **c-d**) Comparison between Slide R blocks on the upper and lower continental slope. The two areas are marked in Fig. 8b. On the upper continental slope in c), longitudinal blocks with a dominant North-South strike are shown as narrow, low-variance features. Slide blocks on the lower continental slope are rotated and relatively small.

Figure 9. Geometric data for blocks in Slides S and R. Slide S blocks are larger in Terrace 4, where they are 1739 m long and 403 m wide on average, with a positive correlation shown on the graph. Slide R blocks in Terrace 5 are 248 m long and 98 m wide on average, showing no

clear correlation on the graphs. The ‘eroded block’ in Fig. 5b was excluded from our analysis, as justified in this work.

Figure 10. Schematic diagrams summarizing the development of MTCs in the study area. **a-c)** the unconsolidated MTC can be remobilized by slope undercutting and a reduction in lateral support. **Stage 1:** During the main phase of Storegga Slide, massive sediments are removed from the southeast side upper continental slope and transported northwestward as MTC 2. Its glide plane eroded the top of the pre-existing MTC 1, generating a group of glide-plane furrows with low sinuosity. Flow channels, such as turbidity and debris, were also developed at this time. **Stage 2:** A local slope failure is sourced on the northwest flank of the Storegga Slide, evacuating the MTCs around Terrace 2. Due to a reduction in its lateral support, the unconsolidated MTC 2 was remobilized, causing its internal channels to become more sinuous. **Stage 3:** Differential compaction in MTC 2 is controlled by structures (furrows) on its glide plane, resulting in the formation of a group of straight grooves on the modern seafloor, which cross-cut the previously formed channels. **d-f)** the instability of laterally spread Slide S blocks was increased and triggered by slope undercutting. **Stage 1:** Together with slide blocks retrogressively spread during Slide S (in Unit 1), the glide plane of the latter slide propagated to the upper continental slope and fragmented the overlying strata. Incipient slabs were generated between the evacuated scarp on the lower continental slope and seafloor cracks on upper slope. **Stage 2:** During the downslope movement of slabs, laterally spread blocks are generated from both their lower and upper boundaries, generating both retrogressively and progressively spread blocks. Compared to the retrogressively spread blocks, these progressive blocks are supported by slabs on the lower continental slope, near which younger and larger blocks are located. **Stage 3:** Recurrent slope undercutting removed lateral support to deposited MTCs that include progressive blocks, triggering the reactivation

of Slide S blocks, which were supported during Stage 2. Stage 3 deformation is documented as seafloor faults, scarps and slumps overlying blocks.

Figure 1

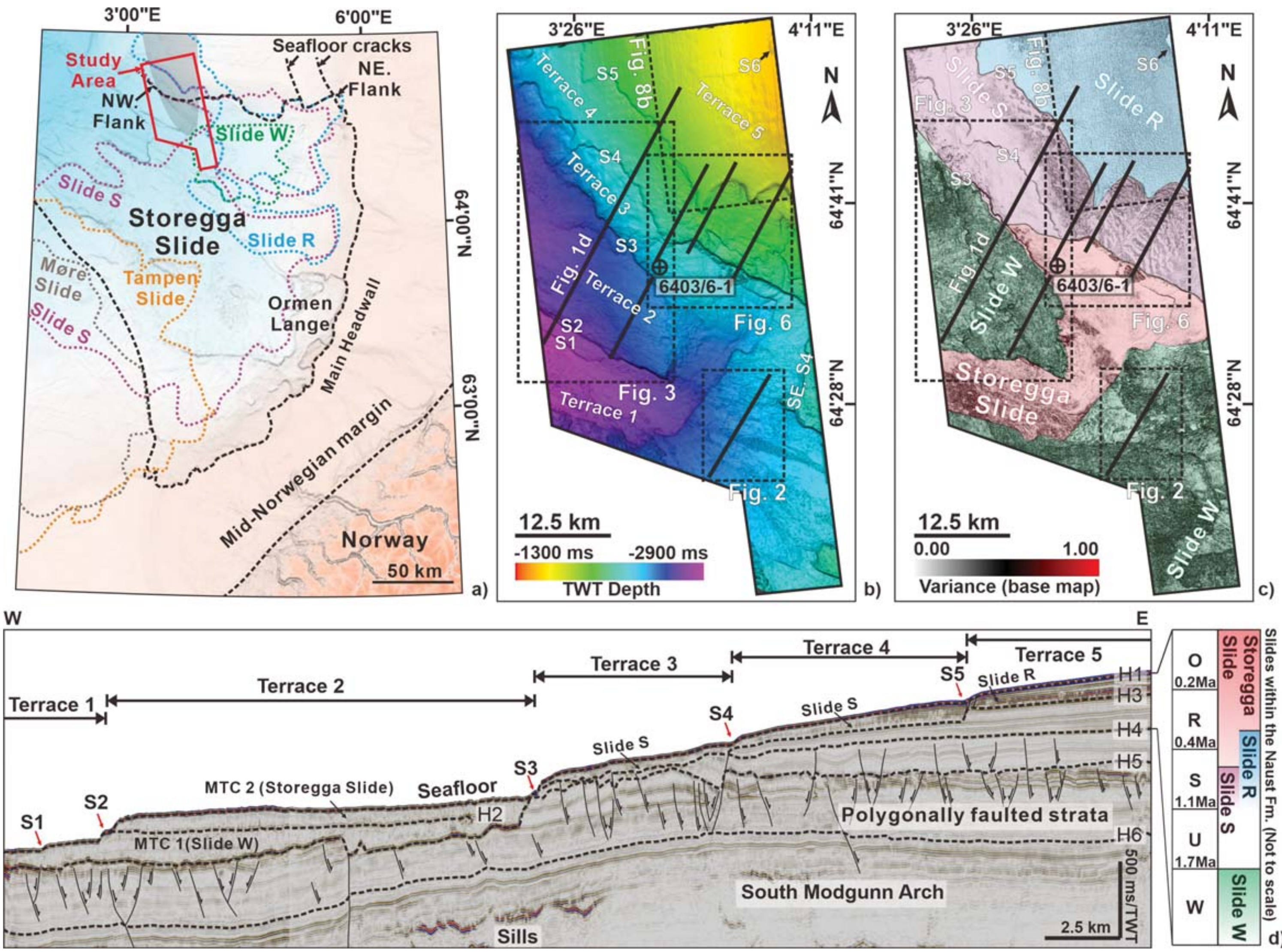

3'00"E
6'00"E
Seafloor cracks
Study Area
NW. Flank
NE. Flank
Slide W
Slide S
Storegga Slide
Slide R
Møre Slide
Tampen Slide
Ormen Lange
Main Headwall
Mid-Norwegian margin
Norway
50 km
64'00"N
63'00"N
a)
3'26"E
4'11"E
Fig. 8b
S5
S6
Terrace 4
Terrace 5
S4
Terrace 3
S3
Fig. 1d
Terrace 2
6403/6-1
Fig. 6
S2
S1
Fig. 3
Terrace 1
SE. S4
Fig. 2
N
64'41"N
64'28"N
12.5 km
-1300 ms
-2900 ms
TWT Depth
b)
Slide S
Slide R
Fig. 3
Slide W
Storegga Slide
0.00
1.00
Variance (base map)
c)
W
E
Terrace 1
Terrace 2
Terrace 3
Terrace 4
Terrace 5
S1
S2
S3
S4
S5
Slide R
Slide S
MTC 2 (Storegga Slide)
Seafloor
H2
MTC 1(Slide W)
Polygonally faulted strata
South Modgunn Arch
Sills
H1
H3
H4
H5
H6
500 ms/TWT
2.5 km
O
0.2Ma
R
0.4Ma
S
1.1Ma
U
1.7Ma
W
Storegga Slide
Slide R
Slide S
Slide W
Slides within the Naust Fm. (Not to scale)
d)

Figure 2

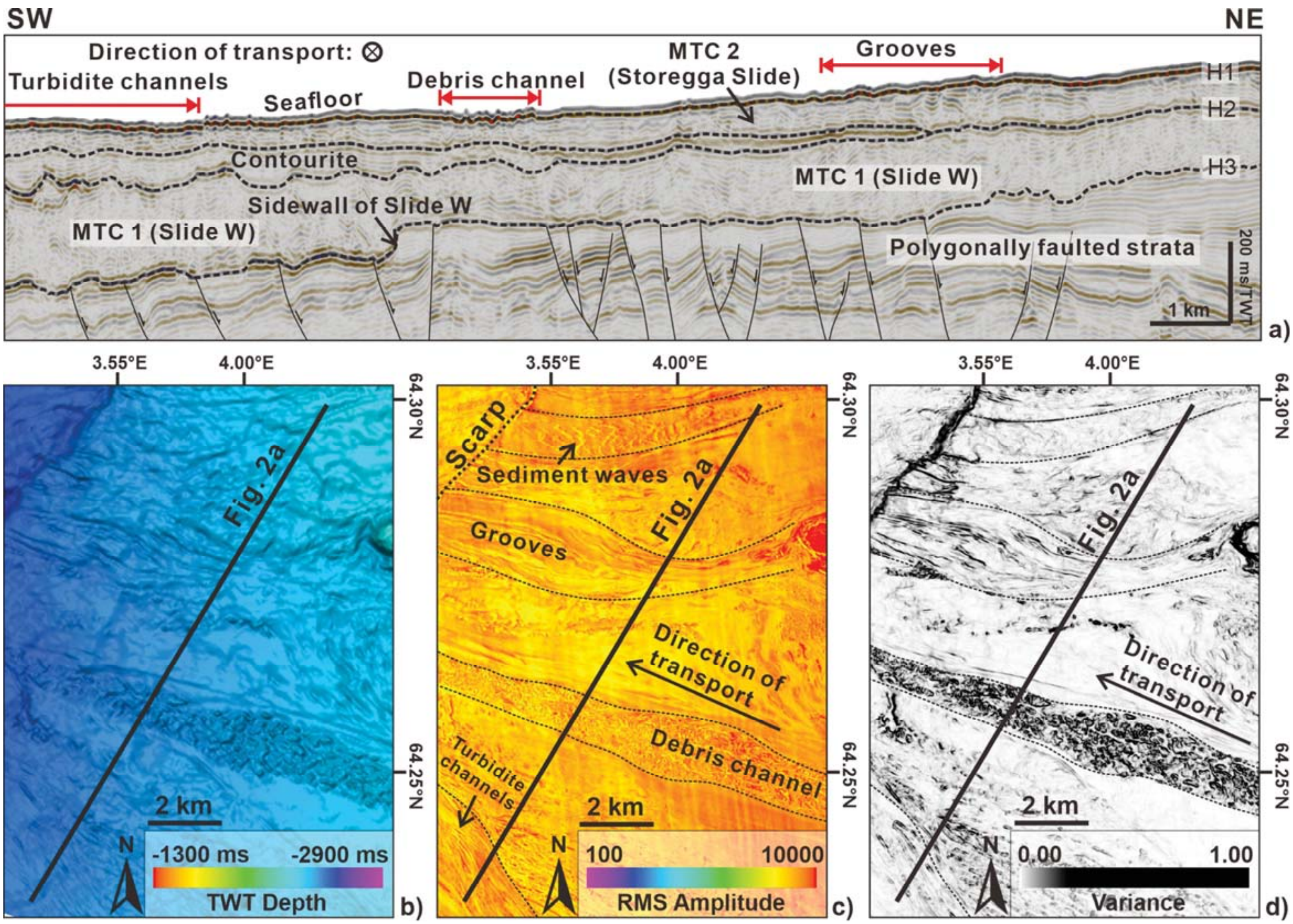
SW
NE
Direction of transport: ⊗
Turbidite channels
Seafloor
Debris channel
MTC 2
(Storegga Slide)
Grooves
H1
H2
H3
Contourite
MTC 1 (Slide W)
Sidewall of Slide W
MTC 1 (Slide W)
Polygonally faulted strata
200 ms TWT
1 km
a)
3.55°E
4.00°E
64.30°N
64.25°N
Fig. 2a
2 km
N
-1300 ms
-2900 ms
TWT Depth
b)
Scarp
Sediment waves
Grooves
Direction of transport
Debris channel
Turbidite channels
100
10000
RMS Amplitude
c)
0.00
1.00
Variance
d)

Figure 3

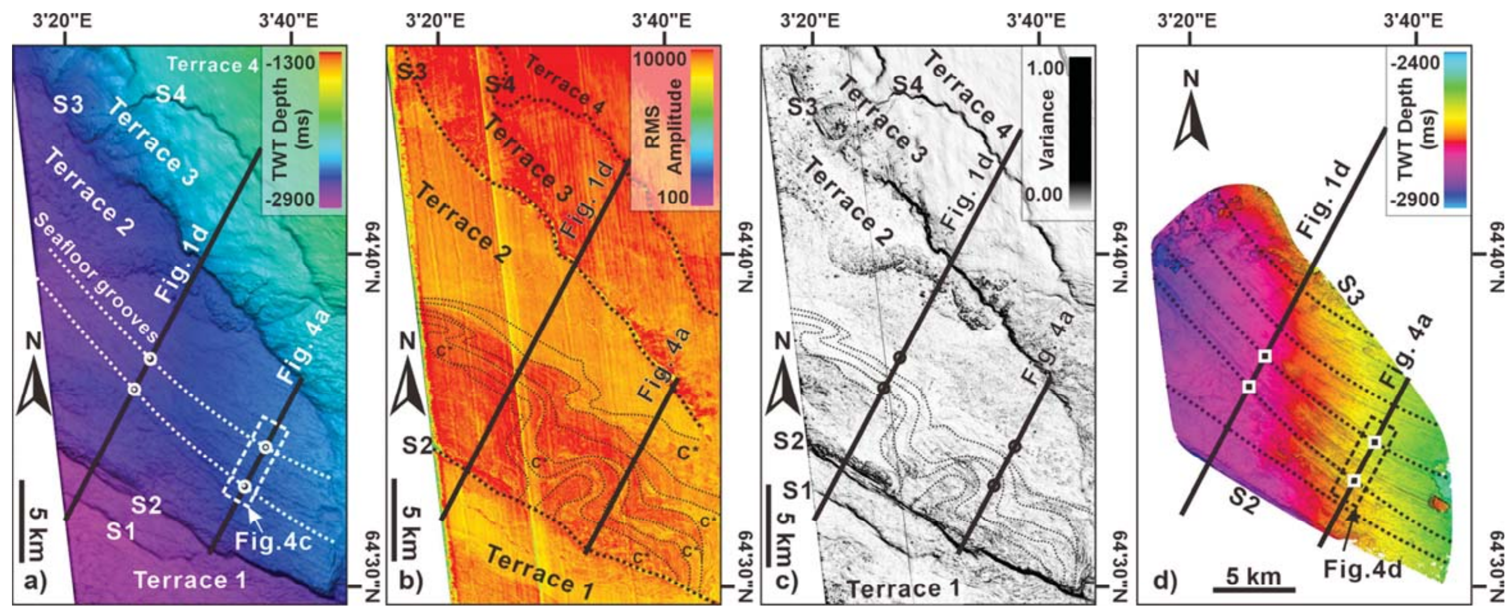
3'20"E
3'40"E
64'40"N
64'30"N
Terrace 4
Terrace 3
Terrace 2
Terrace 1
S1
S2
S3
S4
TWT Depth (ms)
-1300
-2900
Seafloor grooves
Fig. 1d
Fig. 4a
Fig.4c
5 km
N
a)
RMS Amplitude
10000
100
c*
b)
Variance
1.00
0.00
c)
-2400
-2900
Fig.4d
d)

Figure 4

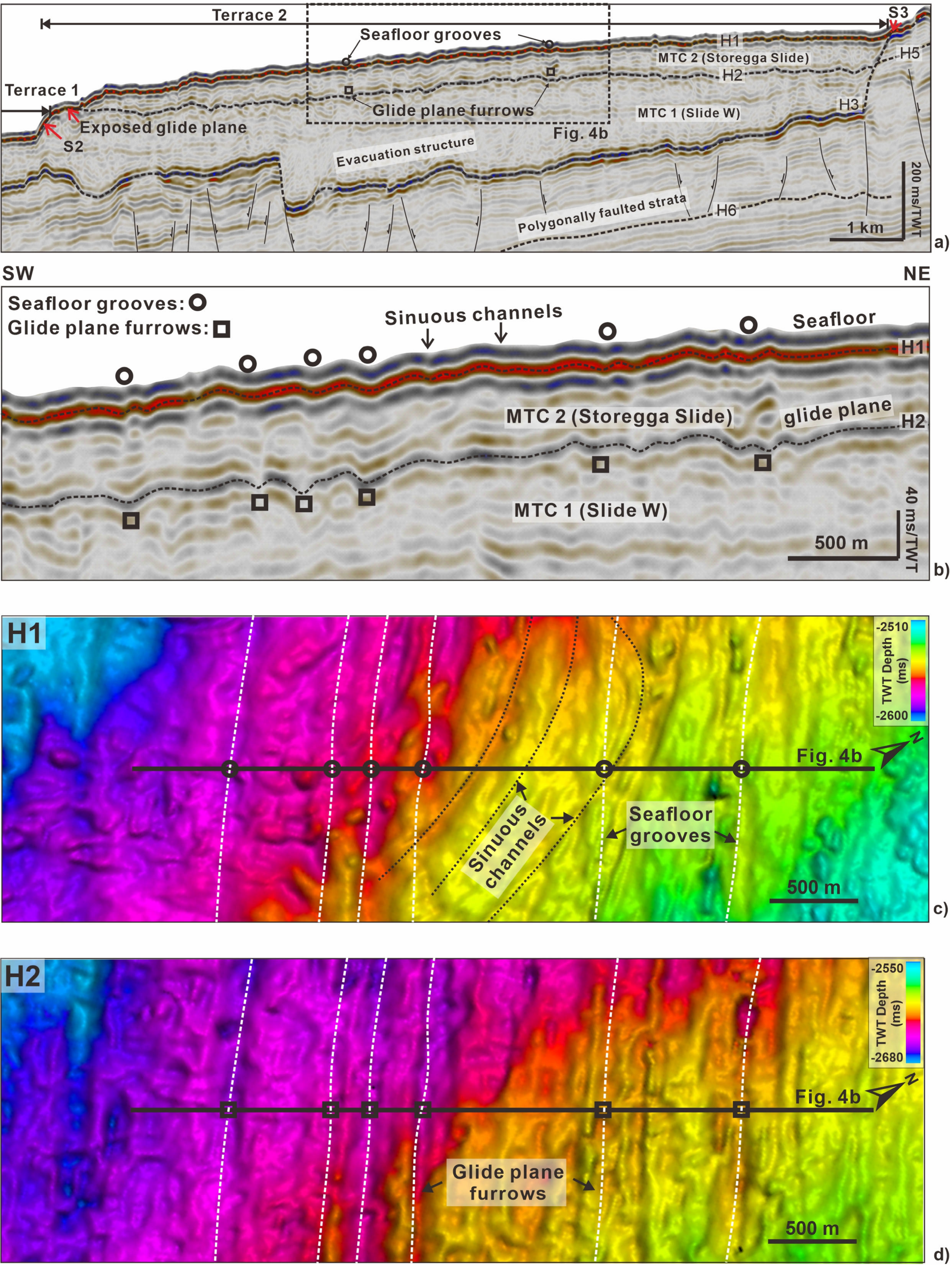

SW
NE
Terrace 2
Seafloor grooves
S3
H1
MTC 2 (Storegga Slide)
H5
H2
Terrace 1
Glide plane furrows
MTC 1 (Slide W)
H3
Exposed glide plane
S2
Fig. 4b
Evacuation structure
200 ms/TWT
Polygonally faulted strata
H6
1 km
a)
SW
NE
Seafloor grooves:
Glide plane furrows:
Sinuous channels
Seafloor
H1
MTC 2 (Storegga Slide)
glide plane
H2
MTC 1 (Slide W)
40 ms/TWT
500 m
b)
H1
-2510
TWT Depth (ms)
-2600
Fig. 4b
N
Sinuous channels
Seafloor grooves
500 m
c)
H2
-2550
TWT Depth (ms)
-2680
Fig. 4b
N
Glide plane furrows
500 m
d)

Figure 5

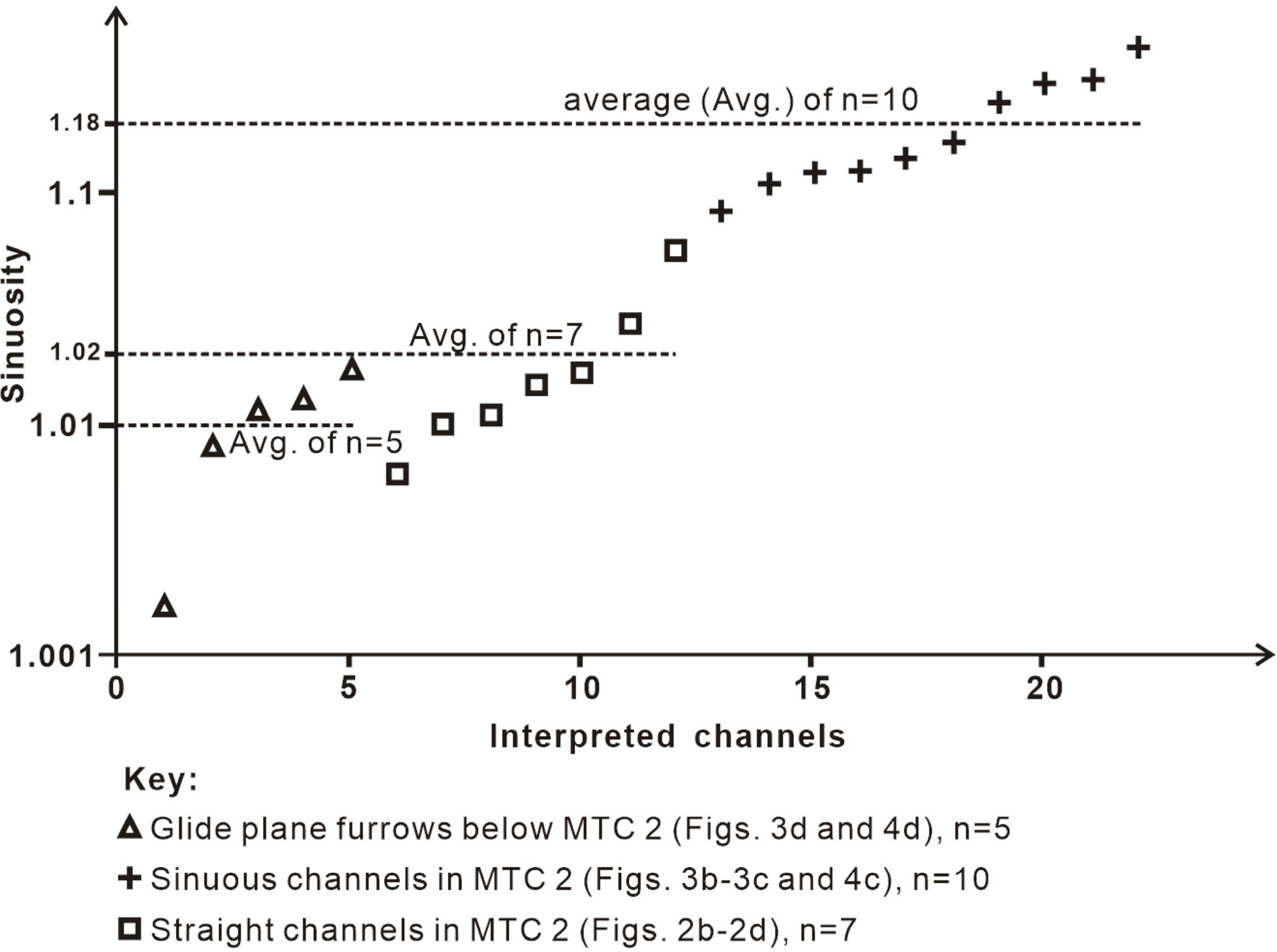

Sinuosity
1.001
1.01
1.02
1.1
1.18
average (Avg.) of n=10
Avg. of n=7
Avg. of n=5
0
5
10
15
20
Interpreted channels
Key:
Glide plane furrows below MTC 2 (Figs. 3d and 4d), n=5
Sinuous channels in MTC 2 (Figs. 3b-3c and 4c), n=10
Straight channels in MTC 2 (Figs. 2b-2d), n=7

Figure 6

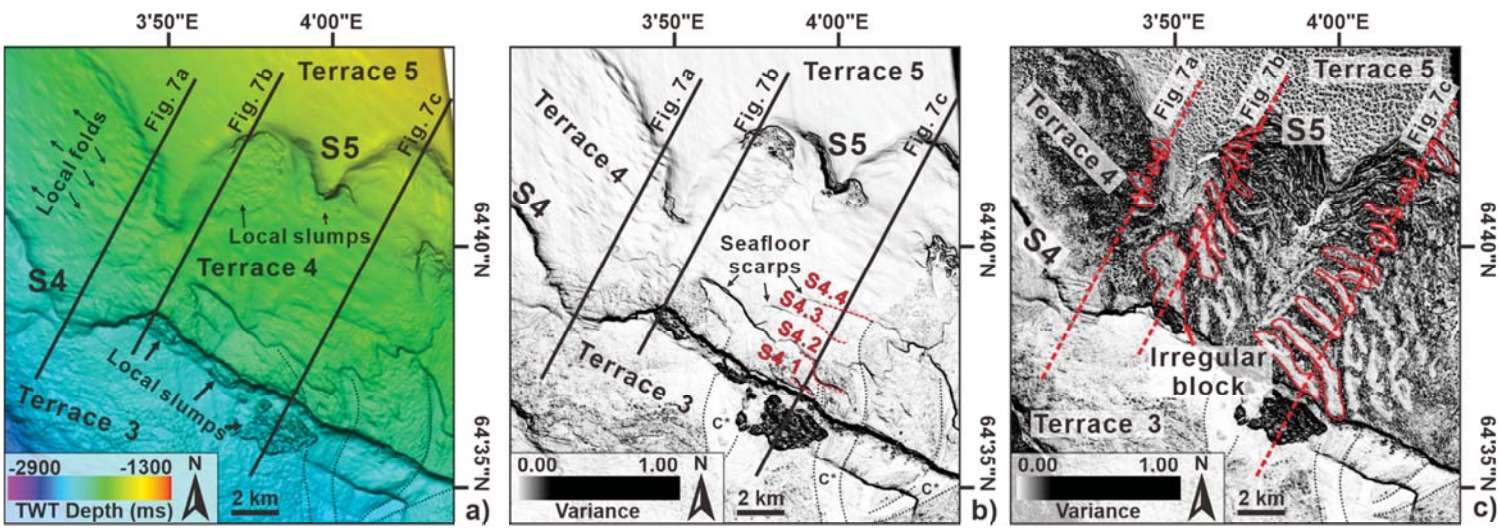

3'50"E
4'00"E
Terrace 5
Fig. 7a
Fig. 7b
Fig. 7c
S5
Local folds
Local slumps
Terrace 4
S4
Local slumps
Terrace 3
64'40"N
64'35"N
-2900
-1300
TWT Depth (ms)
N
2 km
a)
Terrace 4
Seafloor scarps
S4.4
S4.3
S4.2
S4.1
0.00
1.00
Variance
b)
Irregular block
c)

Figure 7

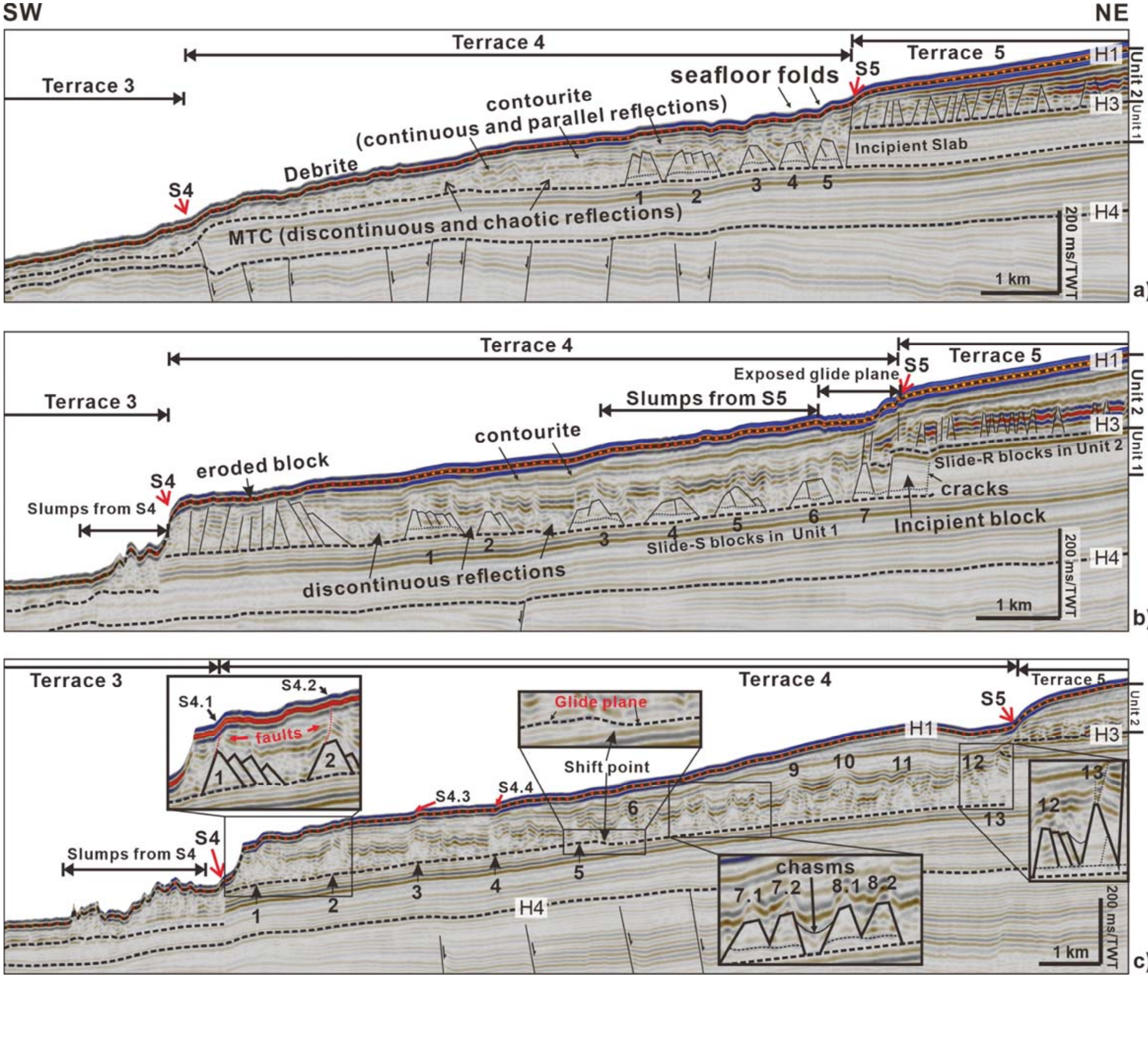
SW
NE
Terrace 3
Terrace 4
Terrace 5
seafloor folds
S5
S4
contourite
(continuous and parallel reflections)
Debrite
MTC (discontinuous and chaotic reflections)
Incipient Slab
H1
H3
H4
Unit 2
Unit 1
200 ms/TWT
1 km
a)
Exposed glide plane
Slumps from S5
eroded block
Slumps from S4
Slide-R blocks in Unit 2
cracks
Incipient block
Slide-S blocks in Unit 1
discontinuous reflections
b)
S4.1
S4.2
faults
S4.3
S4.4
Glide plane
Shift point
chasms
c)

Figure 8

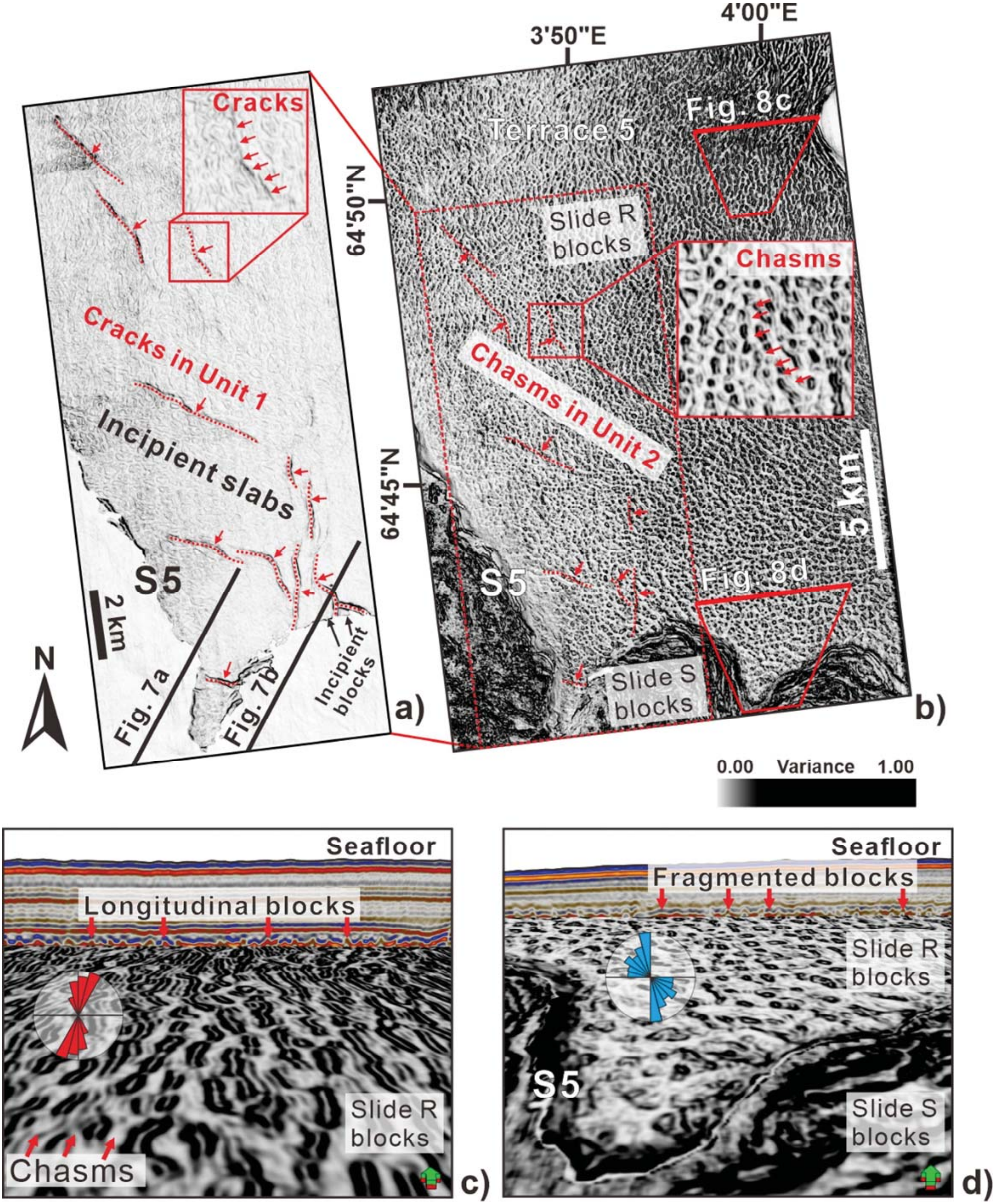

Cracks
Cracks in Unit 1
Incipient slabs
S5
2 km
N
Fig. 7a
Fig. 7b
Incipient blocks
a)
3'50"E
4'00"E
64'50"N
64'45"N
Fig. 8c
Terrace 5
Slide R blocks
Chasms
Chasms in Unit 2
5 km
S5
Fig. 8d
Slide S blocks
b)
0.00
Variance
1.00
Seafloor
Longitudinal blocks
Slide R blocks
Chasms
c)
Seafloor
Fragmented blocks
Slide R blocks
S5
Slide S blocks
d)

Figure 9

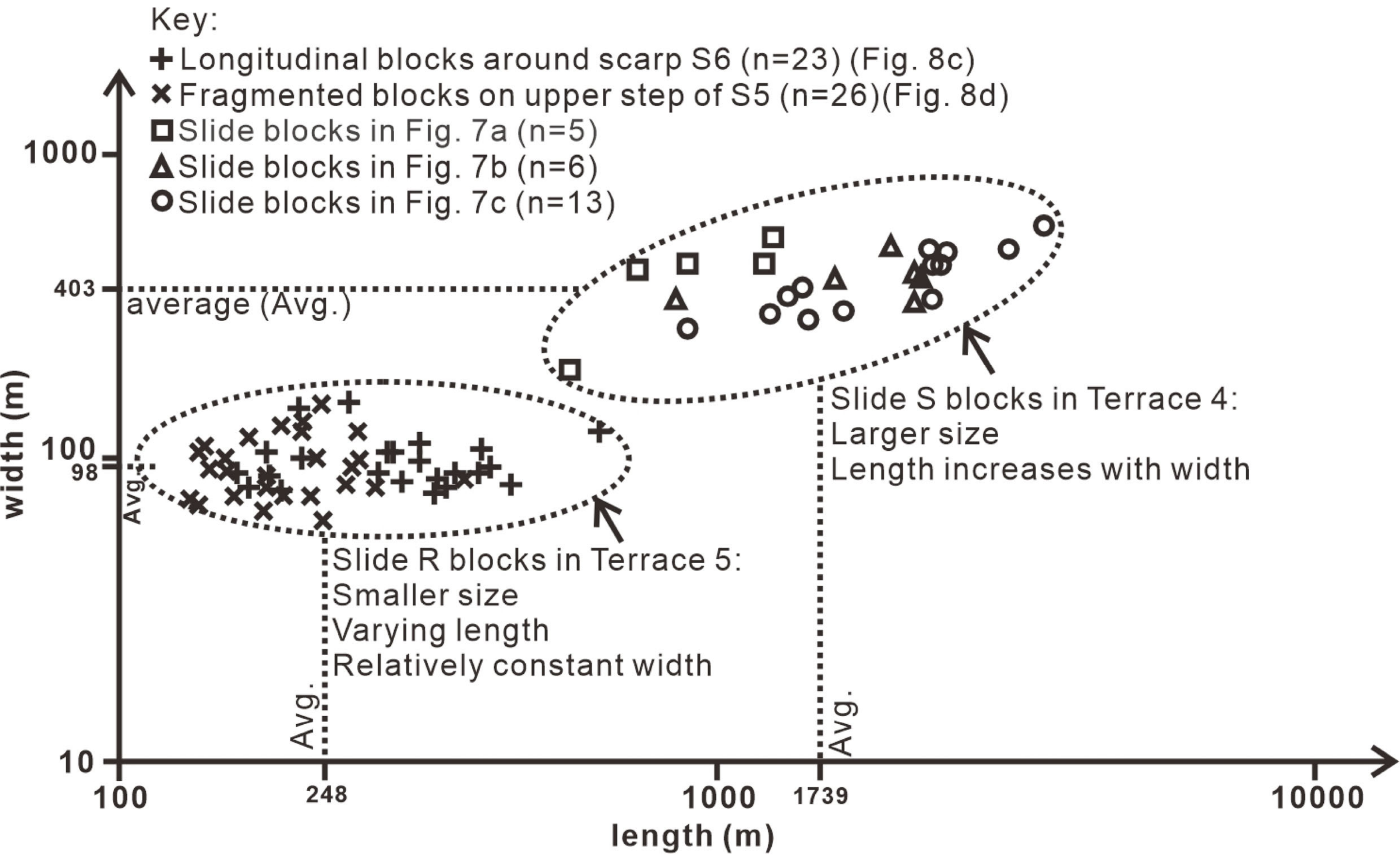

Key:
Longitudinal blocks around scarp S6 (n=23) (Fig. 8c)
Fragmented blocks on upper step of S5 (n=26)(Fig. 8d)
Slide blocks in Fig. 7a (n=5)
Slide blocks in Fig. 7b (n=6)
Slide blocks in Fig. 7c (n=13)
1000
403
average (Avg.)
width (m)
100
98
Avg.
10
Slide S blocks in Terrace 4:
Larger size
Length increases with width
Slide R blocks in Terrace 5:
Smaller size
Varying length
Relatively constant width
Avg.
Avg.
100
248
1000
1739
10000
length (m)

Figure 10

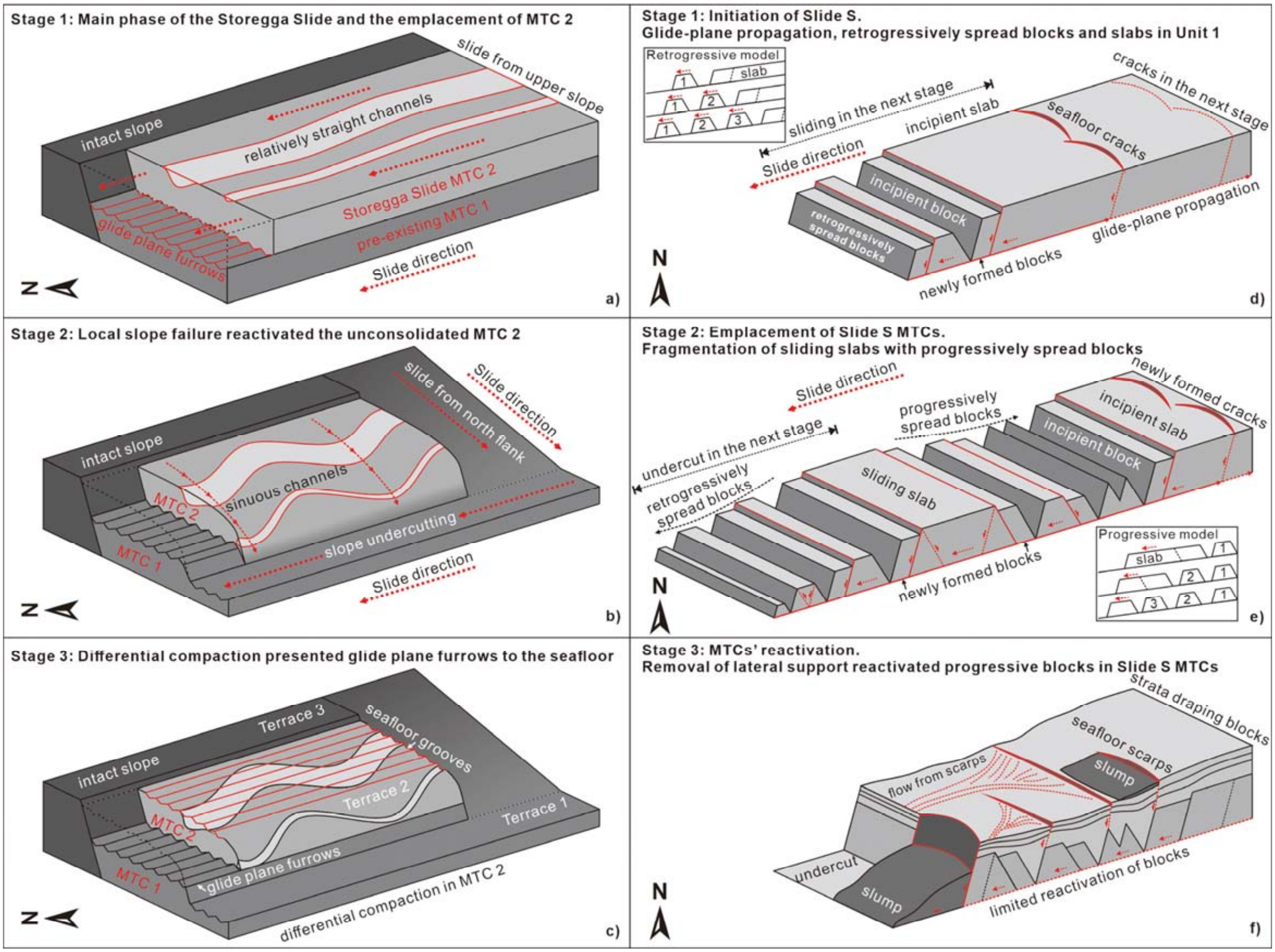

Stage 1: Main phase of the Storegga Slide and the emplacement of MTC 2
slide from upper slope
intact slope
relatively straight channels
Storegga Slide MTC 2
pre-existing MTC 1
glide plane furrows
Slide direction
a)
Stage 1: Initiation of Slide S.
Glide-plane propagation, retrogressively spread blocks and slabs in Unit 1
Retrogressive model
slab
1
2
3
sliding in the next stage
incipient slab
cracks in the next stage
seafloor cracks
Slide direction
incipient block
retrogressively spread blocks
glide-plane propagation
newly formed blocks
N
d)
Stage 2: Local slope failure reactivated the unconsolidated MTC 2
slide from north flank
Slide direction
intact slope
sinuous channels
MTC 2
MTC 1
slope undercutting
Slide direction
b)
Stage 2: Emplacement of Slide S MTCs.
Fragmentation of sliding slabs with progressively spread blocks
Slide direction
newly formed cracks
progressively spread blocks
incipient slab
incipient block
undercut in the next stage
retrogressively spread blocks
sliding slab
newly formed blocks
Progressive model
slab
1
2
3
N
e)
Stage 3: Differential compaction presented glide plane furrows to the seafloor
Terrace 3
seafloor grooves
intact slope
Terrace 2
Terrace 1
MTC 2
MTC 1
glide plane furrows
differential compaction in MTC 2
c)
Stage 3: MTCs' reactivation.
Removal of lateral support reactivated progressive blocks in Slide S MTCs
strata draping blocks
seafloor scarps
flow from scarps
slump
undercut
slump
limited reactivation of blocks
N
f)